optica

Mode-locked mid-infrared frequency combs in a silicon microresonator

Mengjie Yu,[1,2,*] Yoshitomo Okawachi,[1] Austin G. Griffith,[3] Michal Lipson,[4] and Alexander L. Gaeta[1]

[1]Department of Applied Physics and Applied Mathematics, Columbia University, New York, New York 10027, USA
[2]School of Electrical and Computer Engineering, Cornell University, Ithaca, New York 14853, USA
[3]School of Applied and Engineering Physics, Cornell University, Ithaca, New York 14853, USA
[4]Department of Electrical Engineering, Columbia University, New York, New York 10027, USA
*Corresponding author: my2473@columbia.edu

Received 22 April 2016; revised 5 July 2016; accepted 12 July 2016 (Doc. ID 263791); published 29 July 2016

Mid-infrared (mid-IR) frequency combs have broad applications in molecular spectroscopy and chemical/biological sensing. Recently developed microresonator-based combs in this wavelength regime could enable portable and robust devices using a single-frequency pump field. Here, we demonstrate a mode-locked microresonator-based frequency comb in the mid-IR spanning 2.4–4.3 μm. We observe high pump-to-comb conversion efficiency, in which 40% of the pump power is converted to the output comb power. Utilizing an integrated PIN structure allows for tuning the silicon microresonator and controlling cavity soliton formation via free-carrier detection and control. Our results significantly advance microresonator-based comb technology toward a portable and robust mid-IR spectroscopic device that operates at low pump powers.

OCIS codes: (140.3948) Microcavity devices; (190.4975) Parametric processes; (190.4390) Nonlinear optics, integrated optics.

http://dx.doi.org/10.1364/OPTICA.3.000854

1. INTRODUCTION

Optical frequency comb generation using four-wave mixing (FWM) parametric oscillation in microresonators has attracted significant interest [1–12]. Progress in fabrication techniques for low-loss nonlinear devices has led to significant development of comb generation in the mid-infrared (mid-IR) regime [13–19], which is a highly attractive spectral region for applications in molecular spectroscopy and chemical and biological sensing [20]. For example, broadband mid-IR sources, especially from 3 to 4 μm, are useful for breath analysis, since many different species are exhaled, such as carbonyl sulfide, ethane, ethylene, and formaldehyde, which are important biomarkers for various diseases. Mid-IR parametric oscillation and frequency comb generation have been demonstrated in silicon nitride (Si_3N_4) [13], silicon [14,15] microresonators, and crystalline calcium fluoride and magnesium fluoride resonators [17–19]. Various spectroscopic techniques could be enabled by broadband coherent comb sources, including multi-heterodyne and dual-comb spectroscopy, which yield high sensitivity and fast acquisition speeds [21–23].

A critical feature of microresonator-based combs is that they can be mode locked, which results in highly uniform comb spacing across the entire comb. Recently, there have been several demonstrations of such mode locking in the near-infrared regime [9,12,24–28]. To achieve mode locking, the microresonators are pumped in the anomalous group-velocity dispersion (GVD) regime, and soliton formation is controlled via pump frequency detuning with respect to the cavity resonance. Several additional tuning methods have been demonstrated, including pump-power modulation [12], electro-optic tuning based on the Pockels effect [29], and thermal tuning of the cavity resonance [30], which allow for stable, systematic generation of single-soliton states. Soliton formation techniques not involving pump frequency tuning are particularly attractive, since it would allow for the use of ultra-narrow linewidth frequency-stabilized single-frequency pump sources for comb generation and enable simultaneous generation of frequency combs in multiple rings using a single pump source, which would facilitate applications such as chip-scale dual-comb spectroscopy [31].

In this paper, we present the first demonstration of coherent mid-IR frequency comb generation via soliton mode locking in silicon microresonators. The evolution toward temporal cavity soliton formation and mode locking is numerically simulated, including the effects of multiphoton absorption (MPA), free-carrier dispersion (FCD), and free-carrier absorption (FCA). Experimentally, the dynamics are carefully characterized by comb transmission and three-photon absorption (3PA)-induced photocurrent measurements as the pump laser frequency is tuned into a cavity resonance. Mode locking is found to be reproducible at different pump wavelengths and in multiple silicon devices and is repeatedly achievable by appropriate pump tuning. A 40% power conversion from the pump to the mode-locked comb is achieved. Furthermore, we demonstrate full control of the mode-locking dynamics through the electrical tuning of the free-carrier (FC) lifetime, allowing for fixed-pump-frequency

operation. Our results show that the distinct features of silicon, which are high nonlinearity, high thermal conductivity, MPA, and the FC-induced effect, can be suitably exploited for mode-locked broadband mid-IR frequency comb generation.

2. MODE LOCKING VIA PUMP DETUNING

A. Numerical Simulations

We carry out numerical simulations on the nonlinear dynamics of comb generation in silicon microresonators using a modified Lugiato–Lefever model [32–39]. Based on the device structure of the silicon microresonator described in [14], the simulated GVD is anomalous (−102 ps^2/km) for a fundamental TE mode at a pump wavelength of 3.1 μm. Higher-order dispersion, self-steepening, 3PA, and the FC effect (FC lifetime $\tau_{fc} = 100$ ps) are included in the model. Figure 1(a) shows the optical transmission and the effective pump-cavity detuning as functions of pump detuning from the cold cavity resonance. The effective pump-cavity detuning is calculated by subtracting the self-phase modulation, cross-phase modulation, and the FC-induced phase shift from the pump detuning from a cold-cavity resonance. For our simulations, we operate in the under-coupled regime. The evolution of the optical spectra and temporal behavior [Fig. 1(b)] indicates that the soliton state occurs after a transition from a high-noise state and results in high peak power pulses at red effective pump detunings, which coincides with the transmission steps and is consistent with previous observations in other platforms [9,27,30].

Our simulations indicate that the soliton states are achieved at high optical transmissions, corresponding to values close to the off-resonance transmission. This condition is attributed to the high pump power and low pump-to-comb conversion efficiency, which is defined as the soliton power divided by the minimum pump power for soliton formation. In practice, this results in a significant change in the intracavity power when the comb undergoes a transition to the soliton state, resulting in a sudden resonance shift due to thermal effects; this is not included in this model. This thermal shift can affect the allowable range of pump detunings for stable soliton operation, especially in silicon, due to its high thermal conductivity and short heat dissipation time. This issue can be overcome for a given Q-factor and free spectral range (FSR) by operating in the over-coupled regime of the resonator with low pump power. Our simulations show that operating in the over-coupled regime can enhance the output comb power by a factor of 5 as compared to operating in the under-coupled regime and achieves a higher pump-to-comb conversion efficiency. Combined with low pump power, operation in the over-coupled regime results in a smaller change of the absolute intracavity power and thus a smaller thermal shift in the microresonator at the transition to the soliton state. Therefore, operation in the over-coupled regime alleviates the requirements of some complex techniques used in Si_3N_4, MgF_2, and silica microresonators to overcome the transient instability of the states, such as a two-step protocol [12] or searching for an ideal tuning speed of the pump laser [9]. This is consistent with our experimental results shown later.

B. Experimental Demonstration

We use a high-Q etchless silicon microresonator with a silica cladding and an integrated PIN structure, as described in [14]. The

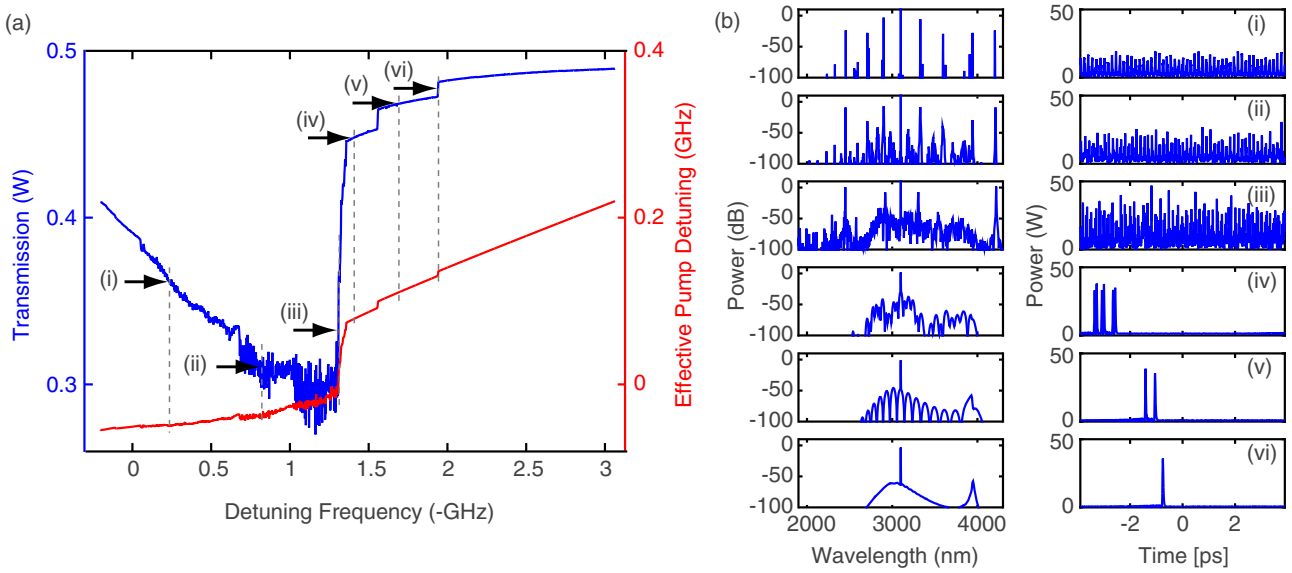

Fig. 1. Numerical simulation of soliton formation via pump laser detuning in a silicon microresonator. (a) Transmission and effective pump-cavity detuning when scanning a pump laser over a cavity resonance. Effective pump-cavity detuning subtracts the resonance shift due to the Kerr effect and free-carrier dispersion from pump detuning. A series of abrupt transmission steps occur in the effective red-detuning regime. (b) Optical spectra and intracavity temporal behavior at different positions (i–vi) in the scan. The plots associated with (i–iii) are in the effective blue-detuning regime, while plots (iv–vi) are in the effective red-detuning regime. The transition to mode locking and soliton formation occurs between (iii) and (iv), as the pump frequency is tuned across the zero effective pump detuning point. As the laser is tuned, (i) primary sidebands are generated through modulation instability and cascaded FWM, (ii) mini-combs are generated around each primary sideband, (iii) with further intracavity power building up, different sets of mini-combs overlap, producing high-noise temporal behavior, (iv) a multiple (6) soliton state occurs with a complex, structured optical spectrum, (v) a 2-soliton state is produced, and (vi) the single soliton state with a smooth optical spectrum is reached. States with different numbers of solitons correspond to the transmission steps shown in (a).

microresonator has an FSR of 127 GHz and is dispersion engineered to have an anomalous GVD beyond 3 μm for the fundamental TE mode. The PIN junction is operated at reverse bias to shorten the effective lifetime of the FCs generated by 3PA and is critical for mid-IR frequency comb generation in silicon [14,39]. The experimental setup is similar to that shown in [15], in which we pump the silicon microresonator with a continuous wave (cw) optical parametric oscillator (Argos Model 2400). The optical spectrum and both the DC and RF components of the extracted 3PA-induced current are monitored simultaneously using an FTIR, a Keithley Sourcemeter, and an RF spectrum analyzer, respectively.

A unique property of silicon microresonator frequency combs is that the intracavity dynamics can be characterized by RF modulation in the PIN junction arising directly from a 3PA-induced photocurrent [15]. Any RF modulation of the optical field is imprinted on the FC density and thus on the photocurrent. Therefore, we are able to examine the comb dynamics using a PIN diode, similar to using a conventional photodiode. The design of this PIN-based detector achieves a high bandwidth as compared with conventional photodiodes due to the short FC lifetime. For example, $\tau_{fc} = 12$ ps is achievable when at a reverse-bias voltage of −15 V, which yields a bandwidth of 13 GHz for this PIN-based detector.

The measured loaded Q-factor of the silicon microresonator is 245,000 at 2.8 μm. The device is over coupled at 2.8 μm, which we verify by measuring a reduced extinction factor when a reverse-bias voltage is applied on the PIN junction and by observing a decreased nonlinear loss due to FCA inside the cavity. We generate frequency combs by tuning the cw pump laser at 2.8 μm into resonance at a reverse-bias voltage of −20 V. The measured threshold power for parametric oscillation is 8 mW, which is consistent with the predicted value based on the Q-factor [40], and the off-resonance pump power in the bus waveguide for soliton mode locking is 35 mW. The comb generation dynamics as the pump power is increased are shown in Fig. 2(b). In Fig. 2 (bi–biii), the pump power builds up inside the microresonator, resulting in an increase in the DC current. During this process, primary sidebands are formed through modulation instability and cascaded FWM. With further power buildup, mini-comb formation occurs near each of the primary sidebands and results in a loss of spectral coherence, creating multiple broad RF beat notes and high RF amplitude noise [Fig. 2(bi–biii)]. Finally, the frequency comb state abruptly transitions to a low-noise state with a more structured optical spectrum [Fig. 2(biv)]. More importantly, the transition coincides with an abrupt increase in the DC current from 0.676 to 0.939 mA, which is a strong indication of pulse formation inside the cavity, since the 3PA-induced current is proportional to the cube of the temporal peak power. In addition, we slowly scan the pump frequency at a 0.1 Hz rate across the resonance while monitoring the transmission using an amplified PbSe detector, as shown in Fig. 2(a). The transmission shows a clear step, which deviates from the expected triangular resonance shape, due to the large Kerr shift induced by intracavity soliton formation [4]; this is predicted by our simulations (Fig. 1). Moreover, the position of the transmission step corresponds to

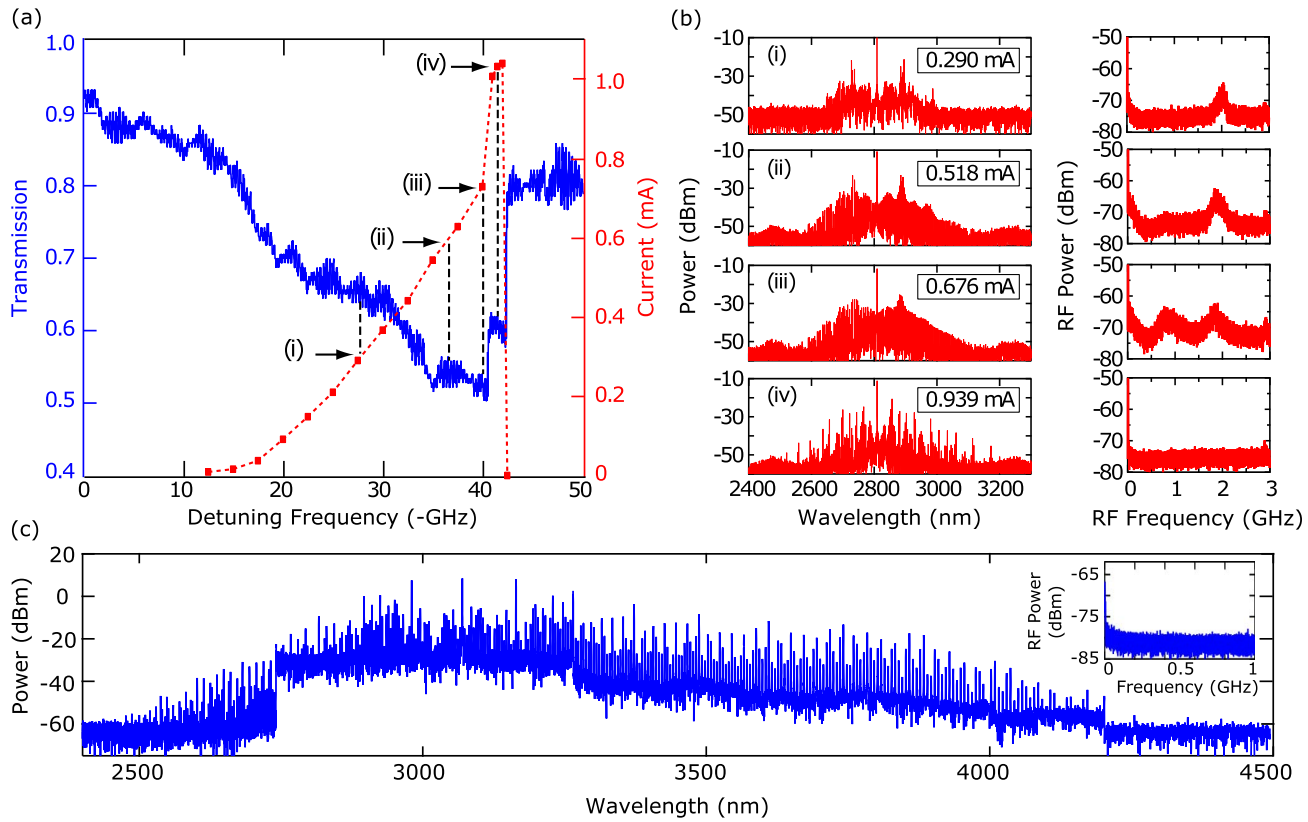

Fig. 2. Evolution toward mode locking via pump frequency detuning from the cavity resonance. (a) Transmission (blue solid curve) and 3PA-induced current (red dashed curve) as the pump frequency is scanned. Arrows correspond to four states (i–iv) in (b). (b) Left: Optical spectrum. Right: RF spectrum of the 3PA-induced current. No RF features are observed from 3 to 10 GHz, which is also within the PIN-based detector bandwidth. (c) Optical spectrum of soliton mid-IR frequency comb pumped at 3.07 μm. Inset: RF spectrum of the 3PA-induced current.

the abrupt change in the current. The fact that the current increases despite the decrease in the intracavity average power is another strong indication of soliton formation.

As discussed previously for other platforms [9,12], the excitation of stable soliton states is often complicated by the thermal nonlinearity of the resonator. Silicon has a large thermal-optic effect in the mid-IR and a large thermal diffusivity (10 times larger than Si_3N_4), which makes the thermal instability in the microresonator more detrimental than in other platforms. Despite the thermal effect, the final multi-soliton state can be reached with a slow scanning speed and can be repeatedly achieved by manually tuning the pump laser. This is attributed to operating in the over coupled regime with a relatively low pump power, where soliton formation can still be achieved due to the large nonlinearity of silicon. Further optimization of the parameters to reduce the transient thermal instability may allow for the observation of multiple soliton steps. In our case, the number of observable steps is limited by the response of the lock-in detection and the scanning speed of the pump laser. In addition, a single soliton state can be potentially achieved by further overcoming the thermal effect, for example, by backward tuning the pump from a multi-soliton state [28] or by thermal control [30].

Next, we obtain a mode-locked mid-IR frequency comb with a near-octave spanning spectrum spanning 2.4–4.3 μm by pumping at 3.07 vm with 80 mW in the bus waveguide [Fig. 2(c)]. In the frequency domain, the comb spans from 70 to 121 THz, which corresponds to more than 400 modes evenly spaced by 127 GHz and covers a bandwidth of 4/5 of an octave. The high wavelength side of the frequency comb is capped at 4.3 μm, which is due to the intrinsic loss in the silica cladding and air absorption (primarily due to CO_2). A higher pump power to achieve soliton formation is required, largely due to the slightly lower Q-factor at 3.07 μm. Unlike previously measured soliton spectra, we observe a significantly depleted pump mode, which we attribute to operating in the highly over coupled microresonator. The output comb power excluding the pump mode is 32 mW and comprises 80% of the total output power of 40 mW, which indicates a 40% pump-to-comb efficiency. To our knowledge, it represents the broadest mode-locked frequency comb demonstrated in microresonators.

3. MODE LOCKING VIA ELECTRICAL TUNING

Using pump laser detuning to achieve, control, and stabilize solitons is limiting since tunable lasers typically suffer from frequency jitter, mode hopping, and limited tuning speed. Therefore, in order to enable an ultralow noise frequency comb with long-term stability, an alternative tuning method combined with a fixed frequency pump laser is beneficial. For example, it will allow for interfacing with quantum cascaded lasers (QCLs), which would be a significant step toward a fully integrated operation and for achieving comb generation in multiple microresonators with a single pump. Thermal tuning of a cavity resonance with an integrated heater has recently been achieved [41], and Joshi *et al.* [30] have demonstrated mode locking with this technique. Our approach here is to achieve a mode-locked mid-IR frequency comb in silicon by controlling the FC lifetime. This novel approach takes advantage of the FC plasma dispersion effect, in which the refractive index of silicon has a weak dependence on the electron–hole pair concentration [42]. In silicon, the larger FC density results in a smaller refractive index, which introduces a blue-shifted cavity resonance during comb generation to achieve the red pump-cavity detuning required for mode locking instead of tuning the pump frequency. And we achieve a larger FC density by increasing the FC lifetime [39]. In our devices, the FC lifetime can be controlled by changing the applied reverse-bias voltage on the PIN junction, which has been previously reported in [43], showing a tuning capability from 3 ns to 12.2 ps for reverse-bias values ranging from 0 to −15 V in a similar PIN junction structure. In addition, since the FC lifetime determines the bandwidth of this tuning method, the tuning speed can be much faster than with thermal tuning.

A. Numerical Simulation

We use the modified Lugiato–Lefever model using our silicon device parameters to numerically simulate FC lifetime tuning for mode locking. The 3PA coefficient is 2×10^{-27} m^3/W^2, and the FCA cross section and FCD parameter are 5.88×10^{-21} m^2 and 3.75, respectively, as defined in [39]. The range of FC lifetimes used in our model is within the experimental capability based on the range of applicable reverse-bias voltages. In our simulations, since FCs due to 3PA play a role above a certain intracavity pump power, the frequency combs are first generated via regular linear pump frequency detuning at $\tau_{fc} =$ 100 ps [Fig. 3(i)], which is followed by an increase in FC lifetime to 300 ps while the pump detuning is kept fixed [Fig. 3(ii)]. This results in a change in pump detuning from effective blue detuned to red detuned, along with the evidence of multiple soliton formation. Further increases in the FC lifetime from 300 to 500 ps and then to 1 ns and eventually 2 ns reduce the number of solitons in the cavity [Fig. 3(iii–v)], and the single soliton state with a smooth optical spectrum is achieved at $\tau_{fc} = 2.5$ ns [Fig. 3(vi)]. In addition, our simulations indicate that soliton formation can be achieved at larger pump detuning values for $\tau_{fc} = 100$ ps, which is equivalent to the conventional method of pump laser

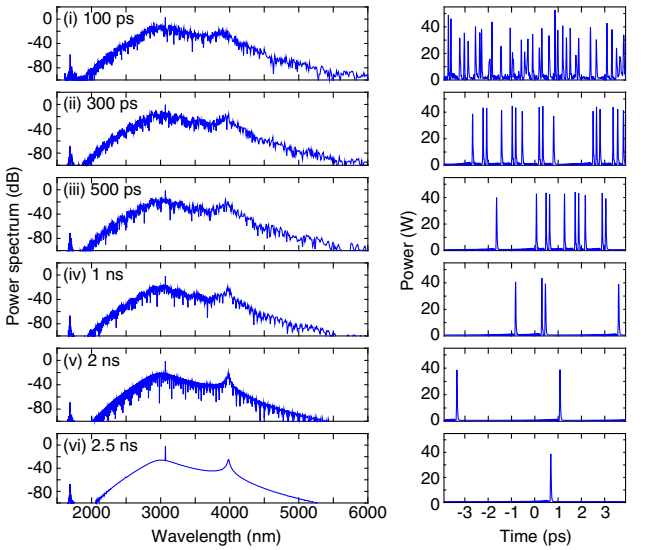

Fig. 3. Numerical simulations of soliton formation via free-carrier (FC) lifetime tuning in a silicon microresonator. Starting with a high-noise state frequency comb, the evolution of the optical spectra (left) and temporal behavior (right) is shown by increasing the FC lifetime from 100 ps to 2.5 ns. The full time axis represents one round trip of the microresonator.

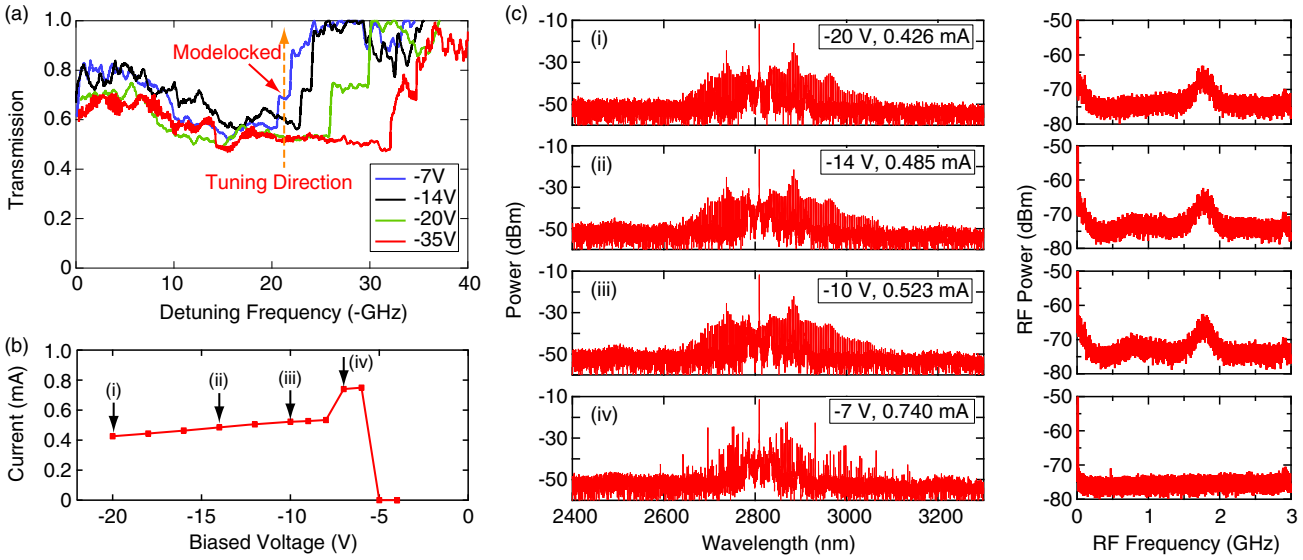

Fig. 4. Electrical tuning of FC lifetime toward mode locking. (a) Optical transmission while scanning the pump frequency over one cavity resonance at different reverse-bias voltages. Orange arrow indicates the voltage tuning path to achieve soliton mode locking, corresponding to the generation dynamics in (c). (b) 3PA-induced current following the tuning path in (a). (c) Comb generation dynamics via electrical tuning. Right: optical spectrum; left: RF spectrum. (i)–(iv) correspond to the various reverse-bias values indicated in (b).

detuning and is due to the fact that such electrical tuning introduces additional nonlinear cavity detuning via FCD. Also, since the FCD relies on the 3PA process, it depends on the dynamical behavior of the intracavity power and changes the FCA-induced nonlinear cavity loss at the same time.

B. Experimental Demonstration

We first investigate the transmission across a cavity resonance by scanning the pump laser frequency for different reverse-bias voltages of −35, −20, −14, and −7 V, as shown in Fig. 4(a). We see that the cavity resonance blue shifts with the decreasing voltage, indicating that we are in a regime where FCD dominates and that, more importantly, tuning the reverse-bias voltage changes the pump detuning from the cavity resonance. Characteristic soliton steps are observed within this voltage range, but not below −6 V, due to the increased FCA. To achieve mode locking, we follow the tuning direction, as shown in Fig. 4(a), from −20 to −7 V, which corresponds to increasing the FC lifetime. Starting from a high-noise state at −20 V, the frequency comb is mode locked at −7 V, corresponding to the position of the soliton step in the transmission. This transition also coincides with an abrupt increase of the 3PA-induced current even at a decreased reverse-bias voltage, which is indicative of intracavity pulse formation [Fig. 4(b)]. The corresponding evolution with both optical and RF spectra is recorded in Fig. 4(c). The final multi-soliton state occurs with a modulated optical spectrum and low RF amplitude noise. There exists multiple voltage tuning paths to achieve mode locking. For example, seen from Fig. 4(a), if the initial reverse-bias voltage is −35 V, the final reverse-bias voltage for mode locking can range from −6 V (the minimum reverse-bias voltage at which mode locking still exists) up to −35 V, depending on the initial pump detuning. Similar behavior is also observed by pumping at 3.07 μm.

C. Stability of Soliton States

Once soliton formation is achieved, we explore the robustness of the soliton state by varying the reverse-bias voltage. Once a particular soliton state is reached, the range over which the reverse-bias voltage can be decreased corresponds to the detuning range of the given soliton step, which, in our case, is from −7 to −6 V. However, soliton states can be quite robust to increases in the reverse-bias voltage. In our experiment, we abruptly increase the reverse-bias voltage from −6 to −20 V and observe that the structured optical spectra, the low noise RF signal, and the high DC current are all maintained (Fig. 5), indicating that the soliton state is preserved. Increasing the reverse-bias voltage is equivalent to reducing the effective red detuning of the pump, which corresponds to lower soliton peak powers [9] and causes the 3PA-induced DC current to decrease from 0.74 to 0.627 mA. As the reverse-bias voltage is gradually decreased from −20 to −10 V, we observe an increase in current due to the same reasoning [Fig. 5(b)]. More interestingly, we observe a hysteresis effect in the measured current, indicating that different cavity detunings are possible even for the same reverse-bias voltage. This is due to the strong dependence of the FC density on the dynamical intracavity power, which also makes it distinct from the thermal tuning technique.

Another feature of electrical tuning is that the DC current is directly linked to the soliton peak power. Since the soliton peak power is determined by the pump-cavity detuning and the resonator properties, we can potentially frequency stabilize the pump-cavity detuning by stabilizing the DC current to a fixed value using the reverse-bias voltage. The response time of electrical tuning can be very fast due to the short FC lifetime and could be four orders of magnitude smaller than thermal tuning response time in Si_3N_4 [44].

4. SUMMARY

In summary, we demonstrate a mode-locked silicon microresonator-based frequency comb with 4/5 of an octave-spanning bandwidth and the low pump power requirement. We achieve a high pump-to-comb conversion efficiency where the output comb

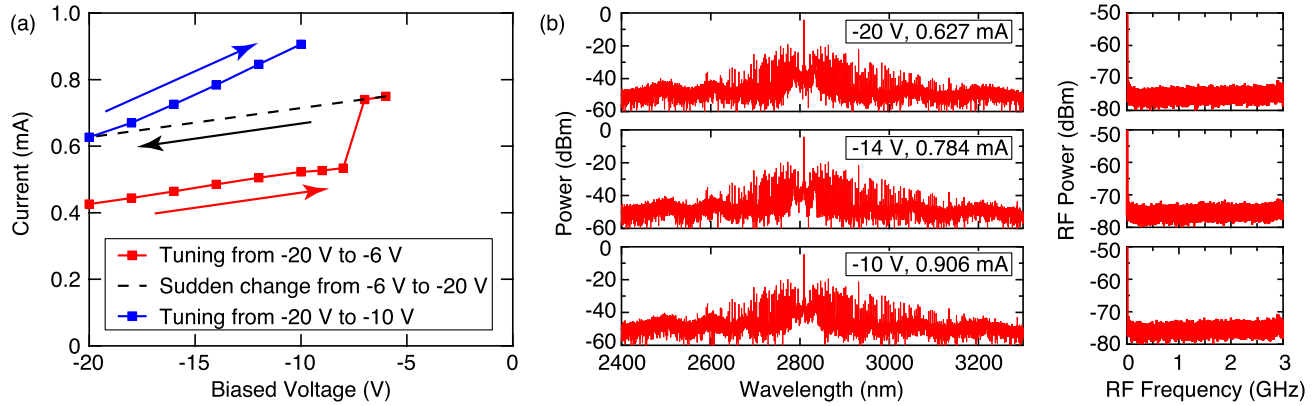

Fig. 5. Electrical measurement and control of the soliton state. (a) DC component of 3PA-induced current measured with a specific reverse-bias voltage tuning path. (b) Optical spectra and RF noise spectra of the soliton state at three reverse-bias voltages corresponding to the blue arrow in (a).

power, excluding the pump mode, is 40% of the total input pump power in the bus waveguide. Mode locking can be achieved without complex laser tuning techniques to overcome transient thermal instability. The electrical measurement and control of FCs in a silicon chip have the potential to greatly simplify the system design for the generation of a highly coherent and stable mid-IR frequency comb. The PIN structure enables the monitoring of the intracavity dynamics and the tuning of the FC lifetime to produce soliton mode locking and to control and stabilize the soliton state with a high bandwidth. Our approach removes the constraints of pump frequency tuning and provides a path toward a fully integrated mid-IR comb source via combining silicon microresonators with mid-IR QCLs and chip-scale dual-comb spectroscopy.

Funding. Intelligence Advanced Research Projects Activity (IARPA); Defense Advanced Research Projects Agency (DARPA) (W31P4Q-15-1-0015); Air Force Office of Scientific Research (AFOSR) (FA9550-15-1-0303); National Science Foundation (NSF) (ECS-0335765, ECCS-1306035).

Acknowledgment. This work was performed in part at the Cornell Nano-Scale Facility, a member of the National Nanotechnology Infrastructure Network, which is supported by the NSF. The authors thank R. K. W. Lau for the useful discussions.

REFERENCES

1. T. J. Kippenberg, R. Holzwarth, and S. A. Diddams, "Microresonator-based optical frequency combs," Science **332**, 555–559 (2011).
2. J. S. Levy, A. Gondarenko, M. A. Foster, A. C. Turner-Foster, A. L. Gaeta, and M. Lipson, "CMOS-compatible multiple-wavelength oscillator for on-chip optical interconnects," Nat. Photonics **4**, 37–40 (2010).
3. Y. Okawachi, K. Saha, J. S. Levy, Y. H. Wen, M. Lipson, and A. L. Gaeta, "Octave-spanning frequency comb generation in a silicon nitride chip," Opt. Lett. **36**, 3398–3400 (2011).
4. T. Herr, K. Hartinger, J. Riemensberger, C. Y. Wang, E. Gavartin, R. Holtzwarth, M. L. Gorodetsky, and T. J. Kippenberg, "Universal formation dynamics and noise of Kerr-frequency combs in microresonators," Nat. Photonics **6**, 480–487 (2012).
5. H. Jung, C. Xiong, K. Y. Fong, X. Zhang, and H. X. Tang, "Optical frequency comb generation from aluminum nitride microring resonator," Opt. Lett. **38**, 2810–2813 (2013).
6. A. A. Savchenkov, D. Eliyahu, W. Liang, V. S. Ilchenko, J. Byrd, A. B. Matsko, D. Seidel, and L. Maleki, "Stabilization of a Kerr frequency comb oscillator," Opt. Lett. **38**, 2636–2639 (2013).
7. S. B. Papp, K. Beha, P. Del'Haye, F. Quinlan, H. Lee, K. J. Vahala, and S. A. Diddams, "Microresonator frequency comb optical clock," Optica **1**, 10–14 (2014).
8. Y. Liu, Y. Xuan, X. Xue, P.-H. Wang, S. Chen, A. J. Metcalf, J. Wang, D. E. Leaird, and A. M. Weiner, "Investigation of mode coupling in normal-dispersion silicon nitride microresonators for Kerr frequency comb generation," Optica **1**, 137–144 (2014).
9. T. Herr, V. Brasch, J. D. Jost, C. Y. Wang, N. M. Kondratiev, M. L. Gorodetsky, and T. J. Kippenberg, "Temporal solitons in optical microresonators," Nat. Photonics **8**, 145–152 (2014).
10. B. J. M. Hausmann, I. Bulu, V. Venkataraman, P. Deotare, and M. Lončar, "Diamond nonlinear photonics," Nat. Photonics **8**, 369–374 (2014).
11. S.-W. Huang, H. Zhou, J. Yang, J. F. McMillan, A. Matsko, M. Yu, D.-L. Kwong, L. Maleki, and C. W. Wong, "Mode-locked ultrashort pulse generation from on-chip normal dispersion microresonators," Phys. Rev. Lett. **114**, 053901 (2015).
12. V. Brasch, M. Geiselmann, T. Herr, G. Lihachev, M. H. P. Pfeiffer, M. L. Gorodetsky, and T. J. Kippenberg, "Photonic chip-based optical frequency comb using soliton Cherenkov radiation," Science **351**, 357–360 (2016).
13. K. Luke, Y. Okawachi, M. R. E. Lamont, A. L. Gaeta, and M. Lipson, "Broadband mid-infrared frequency comb generation in a Si_3N_4 microresonator," Opt. Lett. **40**, 4823–4826 (2015).
14. A. G. Griffith, R. K. W. Lau, J. Cardenas, Y. Okawachi, A. Mohanty, R. Fain, Y. H. D. Lee, M. Yu, C. T. Phare, C. B. Poitras, A. L. Gaeta, and M. Lipson, "Silicon-chip mid-infrared frequency comb generation," Nat. Commun. **6**, 6299 (2015).
15. A. G. Griffith, M. Yu, Y. Okawachi, J. Cardenas, A. Mohanty, A. L. Gaeta, and M. Lipson, "Coherent mid-infrared frequency combs in silicon-microresonators in the presence of Raman effects," Opt. Express **24**, 13044–13050 (2016).
16. R. Shankar, I. Bulu, and M. Lončar, "Integrated high-quality factor silicon-on-sapphire ring resonators for the mid-infrared," Appl. Phys. Lett. **102**, 051108 (2013).
17. C. Y. Wang, T. Herr, P. Del'Haye, A. Schliesser, J. Hofer, R. Holzwarth, T. W. Hänsch, and N. Picqué, "Mid-infrared optical frequency combs at 2.5 μm based on crystalline microresonators," Nat. Commun. **4**, 1345 (2013).
18. A. Savchenkov, V. S. Ilchenko, F. Di Teodoro, P. M. Belden, W. T. Lotshaw, A. B. Matsko, and L. Maleki, "Generation of Kerr combs centered at 4.5 μm in crystalline microresonators pumped with quantum-cascade lasers," Opt. Lett. **40**, 3468–3471 (2015).
19. C. Lecaplain, C. Javerzac-Galy, E. Lucas, J. D. Jost, and T. J. Kippenberg, "Quantum cascade laser Kerr frequency comb," arXiv:1506.00626 (2015).
20. A. Schliesser, N. Picque, and T. W. Hansch, "Mid-infrared frequency combs," Nat. Photonics **6**, 440–449 (2012).

21. F. Adler, P. Maslowski, A. Foltynowicz, K. C. Cossel, T. C. Briles, I. Hartl, and J. Ye, "Mid-infrared Fourier transform spectroscopy with a broadband frequency comb," Opt. Express **18**, 21861–21872 (2010).
22. I. Coddington, W. C. Swann, and N. R. Newbury, "Coherent multiheterodyone spectroscopy using stabilized optical frequency combs," Phys. Rev. Lett. **100**, 013902 (2008).
23. B. Bernhardt, A. Ozawa, P. Jacquet, M. Jacquey, Y. Kobayasho, T. Udem, R. Holzwarth, G. Guelachivili, T. W. Hänsch, and N. Picqué, "Cavity-enhanced dual-comb spectroscopy," Nat. Photonics **4**, 55–57 (2010).
24. M. A. Foster, J. S. Levy, O. Kuzucu, K. Saha, M. Lipson, and A. L. Gaeta, "Silicon-based monolithic optical frequency comb source," arXiv:1102.0326 (2011).
25. K. Saha, Y. Okawachi, B. Shim, J. S. Levy, R. Salem, A. R. Johnson, M. A. Foster, M. R. E. Lamont, M. Lipson, and A. L. Gaeta, "Modelocking and femtosecond pulse generation in chip-based frequency combs," Opt. Express **21**, 1335–1343 (2013).
26. T. Herr, V. Brasch, J. D. Jost, I. Mirgorodskiy, G. Lihachev, M. L. Gorodetsky, and T. J. Kippenberg, "Mode spectrum and temporal soliton formation in optical microresonators," Phys. Rev. Lett. **113**, 123901 (2014).
27. X. Yi, Q.-F. Yang, K. Y. Yang, M.-G. Suh, and K. Vahala, "Soliton frequency comb at microwave rates in a high-Q silica microresonator," Optica **2**, 1078–1085 (2015).
28. M. Karpov, H. Guo, E. Lucas, A. Kordts, M. H. P. Pfeiffer, G. Lihachev, V. E. Lobanov, M. L. Gorodetsky, and T. J. Kippenberg, "Universal dynamics and controlled switching of dissipative Kerr solitons in optical microresonators," arXiv:1601.05036 (2016).
29. H. Jung, K. Y. Fong, C. Xiong, and H. X. Tang, "Electrical tuning and switching of an optical frequency comb generated in aluminum nitride microring resonators," Opt. Lett. **39**, 84–87 (2014).
30. C. S. Joshi, J. K. Jang, K. Luke, X. Ji, A. Klenner, Y. Okawachi, M. Lipson, and A. L. Gaeta, "Thermally-controlled comb generation and soliton modelocking in microresonators," Opt. Lett. **41**, 2565–2568 (2016).
31. F. Zhu, A. Bicer, R. Askar, J. Bounds, A. A. Kolomenskii, V. Kelessides, M. Amani, and H. A. Schussler, "Mid-infrared dual frequency comb spectroscopy based on fiber lasers for the detection of methane in ambient air," Laser Phys. Lett. **12**, 095701 (2015).
32. L. A. Lugiato and R. Lefever, "Spatial dissipative structures in passive optical systems," Phys. Rev. Lett. **58**, 2209–2211 (1987).
33. M. Haelterman, S. Trillo, and S. Wabnitz, "Dissipative modulation instability in a nonlinear dispersive ring cavity," Opt. Commun. **91**, 401–407 (1992).
34. A. B. Matsko, A. A. Savchenkov, W. Liang, V. S. IlChenko, D. Seidel, and L. Maleki, "Mode-locked Kerr frequency combs," Opt. Lett. **36**, 2845–2847 (2011).
35. Y. K. Chembo and C. R. Menyuk, "Spatiotemporal Lugiato-Lefever formalism for Kerr-comb generation in whispering-gallery-mode resonators," Phys. Rev. A **87**, 053852 (2013).
36. S. Coen and M. Erkintalo, "Universal scaling laws of Kerr frequency combs," Opt. Lett. **38**, 1790–1792 (2013).
37. M. R. E. Lamont, Y. Okawachi, and A. L. Gaeta, "Route to stabilized ultrabroadband microresonator-based frequency combs," Opt. Lett. **38**, 3478–3481 (2013).
38. R. T. Hansson, D. Modotto, and S. Wabnitz, "Mid-infrared soliton and Raman frequency comb generation in silicon microrings," Opt. Lett. **39**, 6747–6750 (2014).
39. R. K. W. Lau, M. R. E. Lamont, Y. Okawachi, and A. L. Gaeta, "Effects of multiphoton absorption on parametric comb generation in silicon microresonators," Opt. Lett. **40**, 2778–2781 (2015).
40. T. Kippenberg, S. Spillane, and K. Vahala, "Kerr-nonlinearity optical parametric oscillation in an ultrahigh-Q toroid microcavity," Phys. Rev. Lett. **93**, 083904 (2004).
41. X. Xue, Y. Xuan, C. Wang, P.-H. Wang, Y. Liu, B. Niu, D. E. Leaird, M. Qi, and A. M. Weiner, "Thermal tuning of Kerr frequency combs in silicon nitride microring resonators," Opt. Express **24**, 687–698 (2016).
42. R. A. Soref and B. R. Bennett, "Electrooptical effects in silicon," IEEE J. Quantum Electron. **23**, 123–129 (1987).
43. A. C. Turner-Foster, M. A. Foster, J. S. Levy, C. B. Poitras, R. Salem, A. L. Gaeta, and M. Lipson, "Ultrashort free-carrier lifetime in low-loss silicon nanowaveguides," Opt. Express **18**, 3582–3591 (2010).
44. K. Ikeda, R. E. Saperstein, N. Alic, and Y. Fainman, "Thermal and Kerr nonlinear properties of plasma-deposited silicon nitride/silicon dioxide waveguides," Opt. Express **16**, 12987–12994 (2008).